JOURNAL OF CATALYSIS 139, 494–509 (1993)

Methane Oxidation over Palladium on Zirconia Prepared from Amorphous Pd_1Zr_3 Alloy

P. E. MARTI,* M. MACIEJEWSKI,† AND A. BAIKER†,[1]

*Department of Combustion Technology, Paul Scherrer Institut, CH-5232 Villigen PSI, Switzerland; and †Department of Chemical Engineering and Industrial Chemistry, Swiss Federal Institute of Technology, ETH-Zentrum, CH-8092 Zürich, Switzerland

Received July 13, 1992; revised November 24, 1992

Catalysts for methane oxidation have been prepared by oxidation of amorphous Pd_1Zr_3 metal alloy under different conditions. A sequence of chemical and morphological changes occurring during the alloy oxidation process leads to highly active microporous palladium/zirconia catalysts suitable for the deep oxidation of methane. Depending on the activation temperature, distinct PdO species interacting with zirconia exist in these catalysts, as revealed by oxygen desorption and thermoanalytical measurements. Smaller PdO species strongly interacting with zirconia were found to decompose at a markedly higher temperature than larger PdO species, which only interact weakly with the support. Kinetic studies were carried out in a fixed-bed microreactor at temperatures of 400–800 K and atmospheric pressure using a reactant mixture with a ratio $CH_4:O_2 = 1:4$. Turnover frequencies, based on the exposed palladium surface atoms determined by CO chemisorption, were more than two times higher than those of palladium on zirconia catalysts prepared by impregnation or by coprecipitation. Methane oxidation measurements carried out over the conventionally prepared palladium/zirconia catalysts and a corresponding catalyst derived from Pd_1Zr_3 showed CO and H_2 selectivities higher than 90% under reducing conditions, i.e., with a reactant ratio $CH_4:O_2 = 8:1$ at 870 K.

INTRODUCTION

The catalytic combustion and the oxidative coupling of methane to higher hydrocarbons both have potential large-scale application. The catalytic combustion of hydrocarbons generally is considered an efficient method for reducing the thermal NO_x production. This results from the ability of catalytic combustors to carry out complete oxidation at low fuel concentration, which enables them to operate at lower temperatures. The thermal NO_x concentration can be minimized by this means (*1*, *2*). Catalytic combustion devices have been developed for applications in domestic heating systems, exhaust systems, industrial boilers, and stationary gas turbines (*3*, *4*). Independent of the application, catalysts capable of igniting fuel/air mixtures at the lowest possible temperature are required. Several studies showed that palladium is one of the most active catalysts for the total oxidation of methane (*5–7*). However, the support can influence the ability of palladium to adsorb oxygen and thereby affect its catalytic activity (*8*). It has been found that methane oxidation over supported palladium under oxygen-rich conditions is a structure-sensitive reaction (*6*, *9*).

Another interesting application for methane is its conversion to higher hydrocarbons or methanol. However, the partial oxidation of methane to these products is well known to be a difficult process. An alternative route is partial oxidation to syngas, which can be used as feedstock for Fischer–Tropsch reactions. High yields of CO and H_2 have been reported (*10*) for the selective oxidation of methane on alumina-supported palladium.

[1] To whom correspondence should be addressed.

0021-9517/93 $5.00

In the past decade, considerable interest has been devoted to the potential application of amorphous metal alloys as catalyst precursors (*11–14*). Recently, it has been shown (*14*) that highly active CO oxidation catalysts can be prepared from an amorphous Pd_1Zr_2 metal alloy in *in situ* activation, i.e., by exposure of the alloy to CO oxidation conditions.

The aim of this work is to investigate the potential of palladium/zirconia catalysts prepared from amorphous Pd_1Zr_3 alloy for methane oxidation under both methane-rich and principally lean conditions, and to compare their behaviors with those of conventionally prepared zirconia-supported palladium.

EXPERIMENTAL

Catalysts

The amorphous Pd_1Zr_3 used as catalyst precursor was prepared from the premixed melt of the pure metals by rapid quenching using the technique of melt spinning. For use in the catalytic tests, the 5-mm-wide and 20- to 30-μm-thick ribbons so obtained were ground to flakes to 500- to 200-μm size under liquid nitrogen. Crystallized Pd_1Zr_3 alloy was prepared from amorphous Pd_1Zr_3 by heating at 773 K in vacuum for 2 h. Amorphous and crystalline Pd_1Zr_3 were used as catalyst precursors. Catalysts prepared from the amorphous precursor by *in situ* activation are referred to as a-*T*-is and those prepared by exposure to air as a-*T*-air, where *T* indicates the temperature (K) of treatment. Correspondingly, catalysts prepared from crystalline Pd_1Zr_3 are referred to as c-*T*-is or c-*T*-air, respectively.

As a first reference, a 5 wt% Pd on ZrO_2 catalyst was prepared by impregnation of zirconia with an aqueous solution of $(NH_4)_2PdCl_4$ (Fluka, puriss) using the incipient wetness technique. Zirconia was prepared by precipitation of zirconium dinitrate oxide, obtained from Alfa Products, with a 2.8 *M* aqueous solution of tetramethyl ammonium hydroxide (Fluka, pract.). Prior to depositing palladium, zirconia was calcined in air for 2 h at 773 K. Subsequent to drying for 18 h at 403 K, the precursor was calcined in air at 773 K for 2 h and reduced in hydrogen for 2 h at 573 K.

As a second reference, a palladium/zirconia catalyst, with a molar ratio Pd : Zr of 1 : 3, was prepared by calcination of the water-insoluble hydroxides, followed by reduction. Palladium chloride (20 mmol) obtained from Fluka, and zirconium dinitrate oxide (60 mmol) were dissolved in a HCl solution (0.16 *M*, 250 ml). The solution was added dropwise together with an aqueous solution of tetramethyl ammonium hydroxide (2.8 *M*) to 250 ml of deionized water at 343 K and at a constant pH of 8.5, with vigorous stirring. The product gel was separated from the liquid by centrifugation and washed four times with warm, deionized water (200 ml). Preliminary drying in a stream of air at room temperature was followed by drying at 303 K for 18 h. Final calcination was carried out in air at 773 K for 2 h. The sample was reduced in hydrogen at 523 K. The amount of palladium in the catalyst was determined by TG analysis, decomposing at high temperatures the PdO present in a sample that was first fully oxidized in air. The palladium loading of this catalyst was found to be 25.6 wt%. Both reference catalysts were crushed and sieved, and the size fraction from 150 to 500 μm was used for the catalytic tests.

Physicochemical Characterization

The phase identification of the precursors and final catalysts was carried out by powder X-ray diffractometry using a Siemens D5000 diffractometer. Conditions were: Cu$K\alpha$ radiation, 25 mA, 40 kV, Ni-filter, step scan size = 0.009°. The patterns obtained were compared with JCPDS data files. The mean crystallite size of palladium was estimated by using the Scherrer relationship $d_{hkl} = 51\ \lambda/(B \cos \theta)$, where d_{hkl} is the particle diameter (in Å), λ is the wavelength of Cu$K\alpha$ radiation (1.5409 Å), θ is the Bragg angle, and B is the observed peak width at half maximum peak height. As the

value of B is influenced by instrumental factors as well as crystallite size effects, correction concerning the instrumental broadening and $K\alpha$ doublet broadening were made according to the procedure described in Ref. (*15*).

Thermoanalytical investigation was performed using a Netzsch simultaneous thermoanalyzer (STA 409) and a Mettler thermoanalyzer (TA 2000 C). The sample was placed in a platinum sample pan and heated at 10 K/min. High-purity gases passed through the sample chamber at atmospheric pressure. As a reference, α-Al_2O_3 was used.

The fraction of palladium atoms exposed on the surface was determined by CO chemisorption using a conventional glass volumetric adsorption apparatus, equipped with a high-precision pressure gauge (Ruska DDR 6000). Prior to characterization, all samples were reduced in hydrogen at 523 K for 4 h and evacuated at the same temperature 10^{-3} Pa for 13 h. CO adsorption measurements were carried out at 298 K and pressures ranging from 0 to 12 kPa. The measurements included the subsequent steps: (i) measurement of total CO uptake, (ii) evacuation of the sample for 1 h at 298 K and 10^{-3} Pa, and (iii) measurement of CO uptake corresponding to weakly adsorbed molecules. The amount of chemisorbed CO in each adsorbate was calculated as the difference of the two adsorption uptakes. Studies of the CO adsorption using diffuse reflectance FTIR spectroscopy (*16*) revealed that on the catalysts prepared from the Pd–Zr alloys, bridge-bonded CO was the prevalent surface species in a pure CO atmosphere. On the basis of this observation, the palladium surface area was estimated assuming a stoichiometric factor of two for the CO chemisorption and a cross-sectional area of 0.0787 nm^2 for the palladium atom. The dispersion of the palladium was calculated as $D = Pd_s/Pd_{total}$, where Pd_s corresponds to the number of palladium surface metal atoms and Pd_{total} to the total number of palladium atoms in the sample.

BET surface areas were determined by adsorption of nitrogen or krypton at 77 K in the relative pressure range $0.05 \leq p/p^\circ \leq 0.25$, assuming a cross-sectional area of 0.162 nm^2 for the nitrogen molecule and 0.200 nm^2 for the krypton atom. Nitrogen adsorption and desorption isotherms were measured with a Micromeritics Asap 2000 instrument. Krypton adsorption measurements were performed in the same glass apparatus as used for the chemisorption analysis. Prior to the adsorption measurements, the samples were outgassed in vacuum at 423 K for 2 h.

Temperature-Programmed Desorption (TPD) of Oxygen

The oxygen evolution was measured in a flow system. Each sample (0.200 g) was mounted in a fused-quartz microreactor and treated in a stream (300 cm^3/min STP) of 1% methane, 4% oxygen and helium (balance) at 773 K for 1 h. Subsequently the sample was cooled to room temperature in the same atmosphere and heated in a helium stream (300 cm^3/min STP) at a constant rate of 10 K/min. The oxygen desorbed was monitored with an on-line quadrupole mass spectrometer (Balzers GAM 445).

Catalytic Tests under Oxygen-Rich Conditions

Kinetic studies were performed in a continuous fixed-bed microreactor operated at atmospheric pressure. The reactor was a 6.35-mm-o.d. and 4-mm-i.d. stainless-steel tube placed vertically in an electric furnace. The catalyst temperature was measured at the center of the bed by a thermocouple. To preheat the reactant gas and to obtain a uniform velocity profile, quartz wool was placed before and after the catalyst bed. The reactant feed rate was controlled by mass flow controllers (Brooks). Both the inlet and outlet gas compositions were quantitatively analyzed using an on-line quadrupole mass spectrometer. Comparative activity tests were carried out under the following conditions: reactant feed, 1% CH_4 (99.995% purity), 4% O_2 (99.999%), and 95% He

(99.998%); total flow rate, 300 cm^3/min (STP); catalyst load, 0.250 g. The temperature was increased stepwise from 400 to 800 K. Reported activities are steady-state values, measured after steady-state conversion has been attained. After completion of the whole test series, the measurement at 513 K was repeated to confirm the stability of the catalyst activity during the kinetic test. The methane conversion was calculated from a carbon balance: $100 \cdot (1 - P_{CH_4}/(P_{CH_4} + P_{CO_2} + P_{CO}))$, where P_{CH_4}, P_{CO_2}, and P_{CO} are the partial pressures of CH_4, CO_2, and CO, respectively. In all experiments, no CO production was detected under these experimental conditions. The rate of methane consumption was calculated for conversions below 15% from $r = N_{CH_4} \cdot X/W$, where N_{CH_4} (mol/s) is the molar flow rate of methane, W is the catalyst loading (kg), and X is the fractional conversion of methane.

Tests with sample a-698-is and the two reference catalysts were carried out to determine whether the conversion was limited by interparticle mass transport phenomena. The conversion at 520 K stayed the same when the flow rate through the reactor was changed from 150 to 450 cm^3/min at a constant specific space velocity. When different particle sizes (sieve fraction above 500 μm and fraction below 150 μm) were used, the conversion did not change for both reference catalysts, indicating that internal diffusion was not controlling the overall reaction rate. Conventional tests for pore diffusion were impossible to apply to catalysts prepared from amorphous alloys, since the particle size could not be varied in a sufficiently large range due to embrittlement of the samples.

Catalytic Tests under Methane-Rich Conditions

The tests were carried out in the same reactor configuration as described above, but with a fused-quartz reactor (6 mm o.d. and 4 mm i.d.). As standard reaction gas mixture 16.64% CH_4, 2.08% O_2 and He (balance) with a total flow rate of 150 cm^3/min (STP) was used for these experiments. The temperature was increased stepwise from 673 to 973 K. Prior to the measurements, the samples were conditioned under 1% CH_4, 4% O_2 and He (balance) at 673 K for 1 h. It should be mentioned that with these experiments, safety problems can arise, particularly when reactors with geometries leading to back mixing are used. During one experiment at high temperature, the formation of hydrogen together with possible back-mixing effects led to the formation of a detonating oxygen/hydrogen mixture upstream of the catalyst bed.

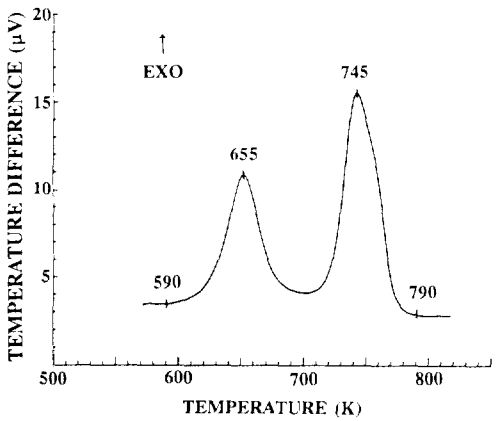

FIG. 1. Thermoanalytical (DTA) investigation of the amorphous Pd_1Zr_3 in argon; sample weight, 100.5 mg; heating rate, 10 K/min. The temperature difference between sample and reference (α-Al_2O_3, 100.0 mg) is expressed in μV for a Pt 10% Rh–Pt thermocouple.

RESULTS

Thermal Behavior of Amorphous and Crystalline Pd_1Zr_3 in Different Atmospheres

To gain information about the structural changes occurring when the amorphous Pd_1Zr_3 alloy is exposed to reaction conditions, we have studied the relevant processes using thermoanalytical methods and X-ray diffraction.

The thermal behavior of the amorphous precursor in argon was examined by DTA (Fig. 1). Under the experimental conditions

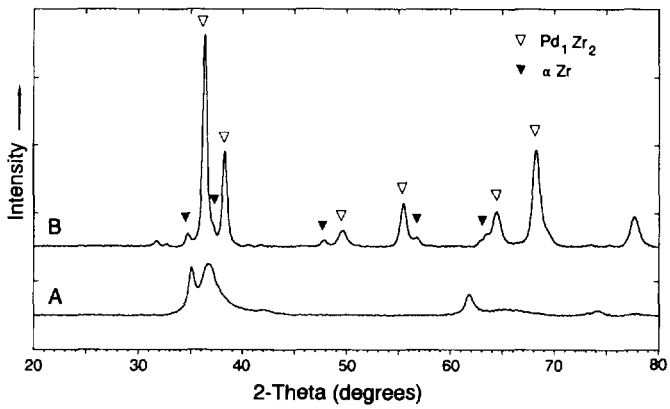

FIG. 2. XRD patterns (Cu$K\alpha$) of the amorphous (A) and crystalline (B) Pd_1Zr_3.

used (heating rate 10 K/min), crystallization takes place in the temperature range 590–790 K. According to the phase diagram of the Pd–Zr system (*17*), amorphous Pd_1Zr_3 after crystallization will be the mixture of two phases: Pd_1Zr_2 and α-Zr. The XRD pattern of the amorphous alloy heated under the same conditions to 650, 700, and 750 K did not indicate any change of the composition of the crystalline product. Thus it appears that the shape of the exothermic crystallization peak (two maxima), shown in Fig. 1, originates from a complex interplay of nucleation, agglomeration, and crystallization and cannot simply be attributed to the separate crystallization of the two phases Pd_1Zr_2 and α-Zr. The XRD pattern of the amorphous alloy after and before crystallization are shown in Fig. 2.

In air, crystallization and oxidation of the amorphous precursor occur simultaneously (Fig. 3A), showing a prominent exothermic peak in the DTA with a maximum at 634 K accompanied by a weight gain. In the case of the crystalline Pd_1Zr_3 (Fig. 3B), two exothermic peaks around 660 and 860 K, respectively, correspond to the oxidation of the material. In the initial phase of the oxidation of the amorphous alloy, the major products found are metallic palladium and zirconia (monoclinic and tetragonal). Metallic palladium originates from the solid-state reduction of PdO with zirconium present in the unreacted core of the alloy, as detailed oxidation and reduction studies of this system revealed (*18*). The small endotherms in the DTA curves around 1120 K, accompanied by a weight loss, are attributed to the decomposition of PdO.

Thermogravimetric measurements performed with the same gas mixture used in

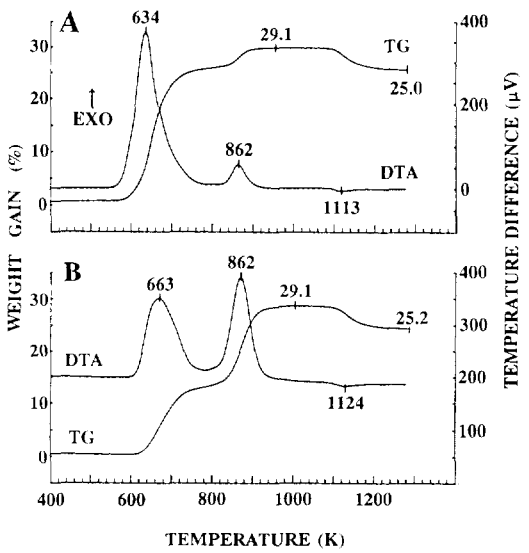

FIG. 3. Thermal stability and oxidation behavior of the amorphous (A) and crystalline (B) Pd_1Zr_3 in air; sample weight, A = 50.3 mg, B = 50.2 mg; heating rate, 10 K/min; reference, α-Al_2O_3, 50.0 mg. Note small endothermal effect of PdO decomposition at (A) 1113 K and (B) 1124 K, respectively.

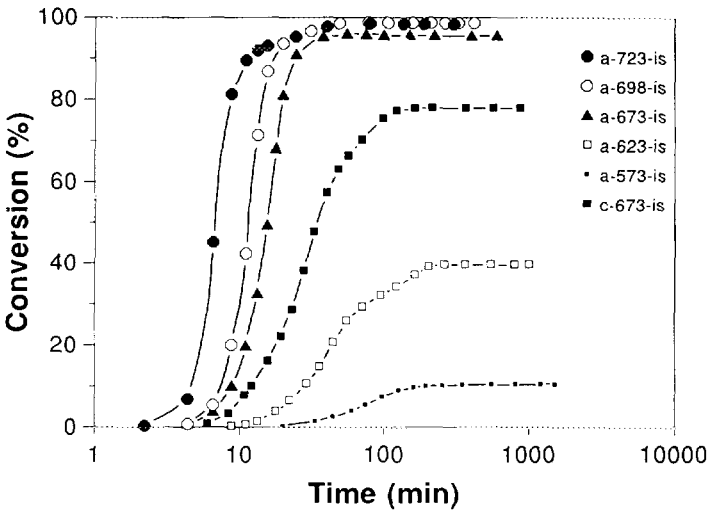

FIG. 4. Change of methane oxidation activity of the amorphous and crystalline Pd_1Zr_3 during *in situ* activation at different temperatures. Catalysts prepared from the amorphous precursor by *in situ* activation are referred to as a-*T*-is and those prepared by exposure to air as a-*T*-air, where *T* indicates the temperature (K) of treatment. Similarly, catalysts prepared from crystalline Pd_1Zr_3 are referred to as c-*T*-is or c-*T*-air, respectively. Reaction gas composition, 1% CH_4, 4% O_2, He (balance); total flow rate, 300 cm^3/min (STP); initial sample weight, 0.2 g.

the activation process (1% CH_4, 4% O_2, and 95% He) and corresponding mixture without methane (4% O_2 and 96% He) revealed that full oxidation of the alloy to PdO/ZrO_2 is only accomplished in the absence of methane in the reactant mixture. In the presence of methane, the simultaneously occurring reduction appears to hinder full oxidation of the alloy, particularly at high temperatures (698 K).

Bulk Structure of Amorphous and Crystalline Precursors after Exposure to Oxidation Conditions

Figure 4 illustrates the change in activity of the amorphous and crystalline Pd_1Zr_3 at different temperatures during their transformation to active catalysts. Both precursors were virtually inactive at the start of the *in situ* activation. After an induction period, the activity developed and reached a steady state reflected by stationary conversion. The development of the activity strongly depended on the temperature of activation. The higher the activation temperature, the shorter the observed induction period.

The changes of the surface morphology after *in situ* activation are illustrated in Fig. 5. The scanning electron micrographs indicate that the initially smooth surface transformed into a rough surface during activation. This phenomenon is further evidenced by an increase of the BET surface area of nearly 1000-fold (Table 1). Regardless of the activation conditions used, the resulting samples were made up of poorly crystalline monoclinic and tetragonal zirconia and palladium oxide, as evidenced by XRD (Fig. 6).

The zirconia phase in the catalyst prepared by coprecipitation remained largely amorphous after calcination at 773 K in air. DTA analysis indicated that crystallization of similarly prepared pure ZrO_2 support occurs already during the calcination procedure (773 K, 2 h), whereas with the PdO/ZrO_2 sample it begins around 870 K, suggesting that PdO enhances the thermal sta-

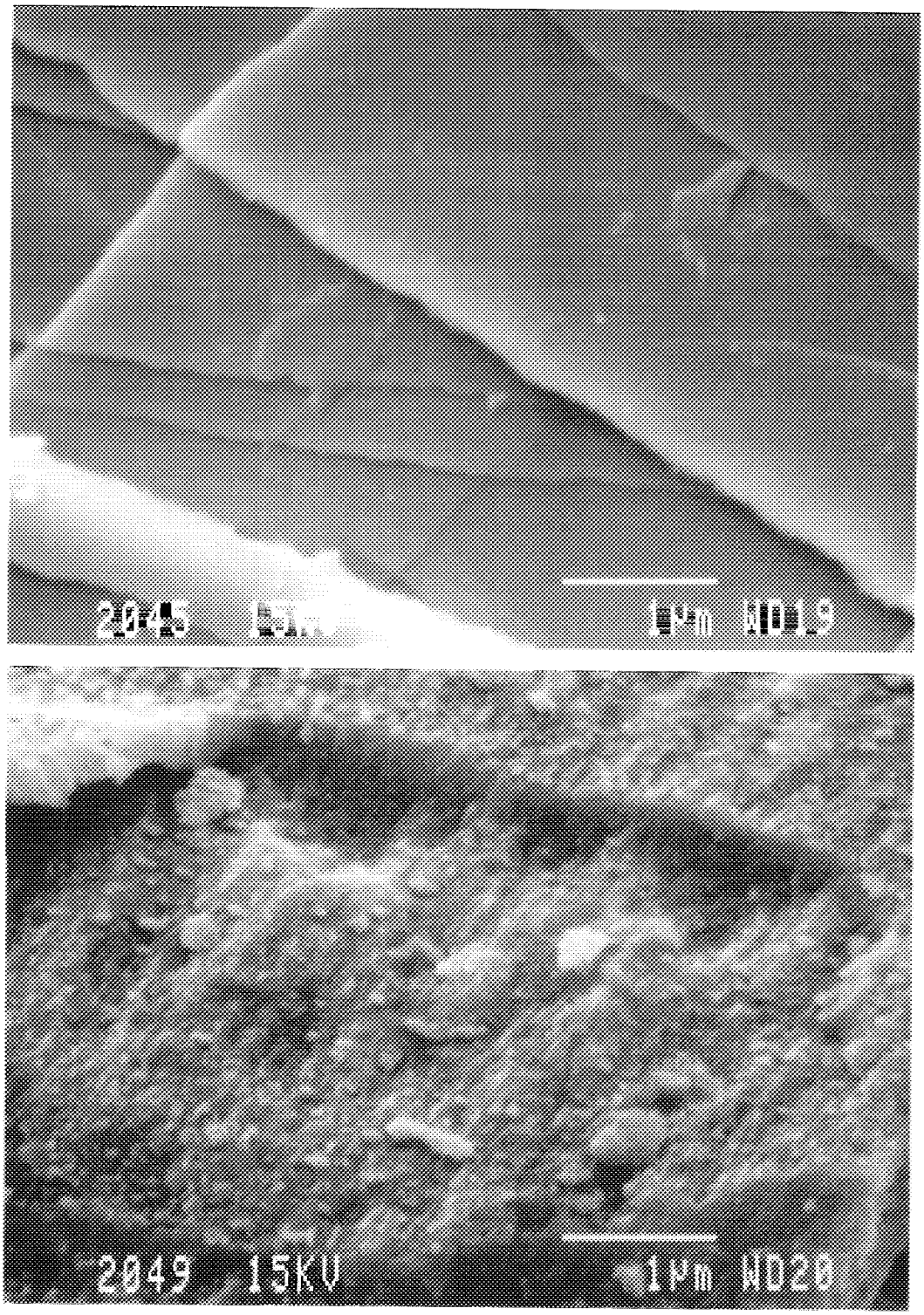

FIG. 5. Scanning electron micrographs of the amorphous Pd_1Zr_3 before (top) and after (bottom) *in situ* activation at 673 K.

TABLE 1

Textural and Morphological Properties of Precursors and Final Catalysts

Catalyst	Surface area BET (m^2/g)	Dispersion[a] (%)	Palladium surface area[a] (m^2/g)
Amorphous Pd_1Zr_3	0.04[b]	—	—
Crystalline Pd_1Zr_3	0.05[b]	—	—
a-573-is	21.4	4.9	4.9
a-623-is	33.6	5.7	5.6
a-673-is	38.5	5.7	5.7
a-698-is	35.5	5.6	5.6
a-723-is	21.8	5.1	5.0
a-573-air	29.0	5.5	5.4
a-623-air	33.4	6.7	6.7
a-673-air	28.1	6.7	6.7
c-673-is	16.0	3.8	3.8
c-623-air	17.2	4.8	4.7
5% Pd/ZrO_2[c,d]	76.0	12.7	2.8
25.6% Pd/ZrO_2[c,e]	119.3	6.3	6.3

Note. Catalysts prepared from the amorphous precursor by *in situ* activation are referred to as a-*T*-is and those prepared by exposure to air as a-*T*-air, where *T* indicates the temperature (K) of treatment. Similarly, catalysts prepared from crystalline Pd_1Zr_3 are referred to as c-*T*-is or c-*T*-air, respectively.

[a] Palladium surface areas and dispersions derived from CO chemisorption measurements.

[b] Measured with krypton.

[c] After 2 h treatment at 723 K in 1% CH_4, 4% O_2, and 95% He.

[d] Prepared by impregnation.

[e] Prepared by coprecipitation.

bility of amorphous zirconia. It is known that the thermal stability of amorphous zirconia can be significantly improved by adding oxides (*19*), and this seems to be true also for PdO. After reduction in hydrogen at 523 K, reflections due to poorly crystalline tetragonal zirconia and small palladium particles were observed in the XRD pattern of this catalyst (Fig. 7A). The XRD pattern of the catalyst prepared by impregnation indi-

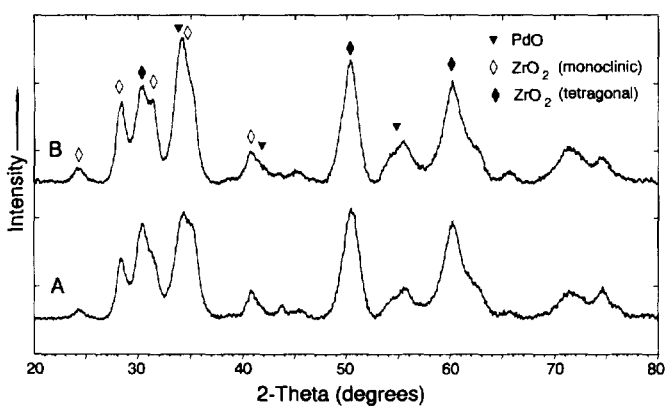

FIG. 6. XRD patterns of catalysts prepared by activation of Pd_1Zr_3 (A) in air (a-623-air) and (B) *in situ* (a-698-is).

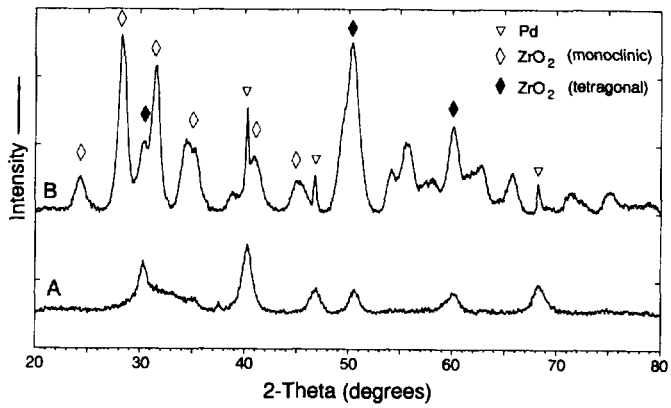

FIG. 7. XRD patterns of the catalyst prepared by coprecipitation (25.6% Pd/ZrO_2) (A) and the catalyst prepared by impregnation (5% Pd/ZrO_2) (B) after reduction in hydrogen.

cated the presence of palladium particles on crystalline zirconia adopting the monoclinic and tetragonal structure (Fig. 7B). The mean crystallite sizes of palladium, calculated from the Scherrer equation using the (111) reflection, were about 30 nm for the catalyst prepared by impregnation, 8 nm for the catalyst prepared by coprecipitation, and 12 nm for the a-698-is catalyst after reduction in hydrogen.

Physisorption Measurements and Palladium Surface Area

BET surface areas, palladium surface areas, and palladium dispersions measured for the different samples are listed in Table 1. BET surface areas as well as palladium surface areas were dependent on the activation conditions and the precursor type. A maximal BET surface of 38 m^2/g was obtained for the catalyst prepared from amorphous Pd_1Zr_3 by *in situ* treatment at 673 K. Activation at higher temperatures led to a drastic decrease of the specific surface area, probably due to micropore collapse occurring during treatment. It is interesting to note that the palladium surface area was less sensitive to the temperature of treatment than the BET surface area.

Nitrogen sorption measurements (nitrogen capillary condensation) yielded for all catalysts prepared from Pd_1Zr_3 type I isotherms, according to the IUPAC classification (*20*), indicating that these materials contained predominantly micropores, independent of the activation procedure used. Only very little hysteresis was observed between adsorption and desorption isotherms in the pressure range typical for mesopores. The *t*-plots (adsorbed volume versus statistical thickness of adsorbed layer) showed the typical deviation from linearity observed for microporous solids (*21*). Both reference catalysts exhibited nitrogen sorption isotherms of type IV, with type H2 hysteresis in the mesopore pressure range.

TPD of Oxygen

Figure 8 depicts the oxygen evolution profiles of samples a-698-is, 5 wt% Pd/ZrO_2, and 25.6 wt% Pd/ZrO_2. The rate of oxygen desorption per mol palladium in the sample is plotted as a function of catalyst temperature. It should be noted that similarly pretreated pure zirconia did not exhibit oxygen desorption up to 1270 K. The TPD profile of the catalyst prepared by impregnation shows the overlapping of two peaks, a prominent one around 900 K followed by a smaller one around 1020 K. The first peak appearing at lower temperature is attributed to the decomposition of bulk PdO, which is only weakly interacting with the zirconia matrix, while the high-temperature desorp-

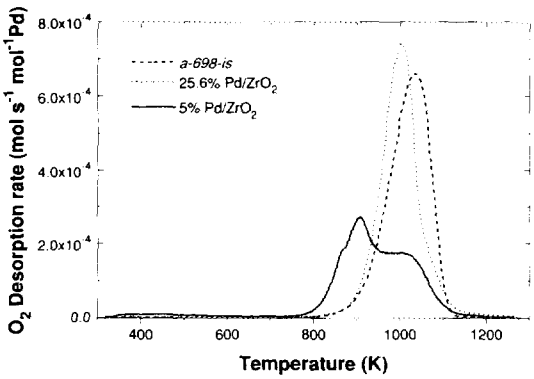

FIG. 8. Temperature-programmed oxygen evolution from catalyst a-698-is and both reference catalysts after treatment in 1% CH_4 and 4% O_2 at 773 K for 1 h. Sample weight, 0.2 g; carrier gas, He (300 cm^3/min); heating rate, 10 K/min.

tion originates from PdO (small particles) interacting strongly with ZrO_2. A similar conclusion was reached by Baldwin and Burch (*22*) for Pd/SiO_2 catalysts by means of TPR. High-temperature peaks in the TPR profiles were associated with a strong interaction between support and small PdO particles,stabilizing them toward reduction.

The catalyst prepared by coprecipitation and the sample a-698-is showed only one desorption peak around 1000 and 1030 K, respectively, indicating that these catalysts contained predominantly PdO species strongly interacting with zirconia. These results also suggest that the PdO–ZrO_2 interaction is slightly stronger in a-698-is than in the 25.6 wt% Pd/ZrO_2 catalyst.

The total amount of desorbed oxygen was calculated by integrating the oxygen desorption rate with time, and results are summarized in Table 2. After exposure of a-698-is and 25.6 wt% Pd/ZrO_2 to the reactant mixture at 773 K, more than 90% of the palladium was present as PdO. In the case of the 5 wt% Pd/ZrO_2 catalyst, only 56% of palladium was in the oxide form, due probably to the inability of the larger palladium crystallites to be oxidized fully under these experimental conditions.

DTA curves of the samples a-573-is and a-698-is, presented in Fig. 9, illustrate the influence of the activation temperature on the decomposition behavior of the PdO constituent in air. The DTA curves reveal a significantly different thermal stability of the PdO phases in these samples. PdO in a-698-is decomposes in a single endothermic step, indicating that the PdO particles have similar interaction with zirconia. In contrast, the two discernible broad endothermic signals (1157 and 1100–1390 K) measured for a-573-is point toward the existence of PdO species with different interaction with ZrO_2. On the basis of the TG and DTG curves (not shown in Fig. 9), the amount of PdO decomposed at higher temperature could be roughly estimated as 60% of the total amount of PdO present in the alloy after activation. The interaction of PdO with zirconia depends on several factors (clustering, segregation, wetting, etc.) that are influenced by the temperature of pretreatment (activation). High temperatures favor the formation of rela-

TABLE 2

Characteristic Data of Oxygen Desorption Measurements

Catalyst	T_{max} (K)	Amount oxygen evolved[a] (μmol)	(mol/mol Pd)
a-698-is	1030	194	0.925
5% Pd/ZrO_2	900	15.9	0.337
	1020	10.4	0.222
25.6% Pd/ZrO_2	1000	198	0.943

[a] Oxygen evolved from 0.2-g sample in the temperature range 700 to 1273 K into 300 cm^3/min He at a heating rate of 10 K/min following treatment at 773 K in 1% CH_4, 4% O_2, and He (balance) for 1 h.

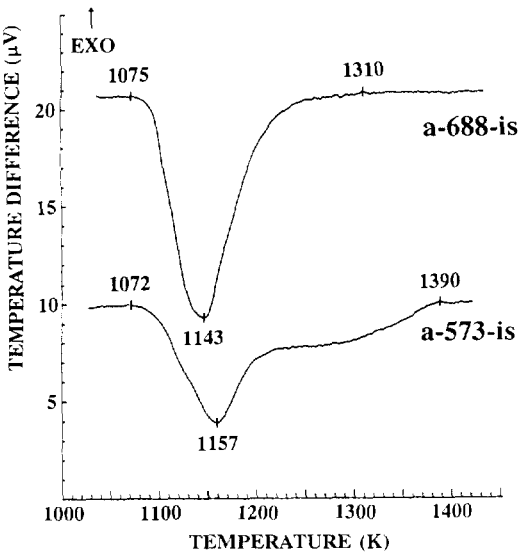

FIG. 9. DTA curves of the decomposition; in air of PdO present in the samples a-698-is (top) and a-573-is (bottom). Sample weight, 86.4 mg of a-698-is and 95.6 mg of a-573-is; heating rate, 10 K/min; reference, α-Al_2O_3, 90.9 mg.

tively large PdO particles interacting less strongly with zirconia.

Catalytic Activity under Oxygen-Rich Conditions

Preliminary tests under these conditions showed that in the reactor filled with quartz wool alone the reaction was negligible at temperatures below 850 K. The activity of pure ZrO_2 was also negligible in the temperature range in which the methane conversion was below 50% (<600 K). However, at 800 K the conversion of methane over ZrO_2 was 0.9%.

The fresh reduced 5 wt% Pd/ZrO_2 exhibited nonlinear behavior in the Arrhenius plot and a significant enhancement of the activity after completion of the kinetic measurements. The mass specific reaction rate (at 520 K) increased by a factor of 14. Part of this enhancement of the activity can be attributed to the fact that the palladium dispersion was two times higher after the kinetic test. A similar behavior has been reported for alumina-supported palladium (*9, 22, 23*). The changes in the activity of the catalysts occurred irrespective of whether the precursor was calcined or calcined and then reduced prior to testing. This enhancement of the activity is attributed to a restructuring of the palladium oxide particles on the support.

Similar behavior, although not so marked, was found for the catalyst prepared by coprecipitation. Because of this, both reference catalysts were treated in the reaction gas mixture at 723 K for 2 h prior to the kinetic measurements.

The temperature dependences of methane oxidation over a-698-is, a-623-air, and the two reference catalysts are presented in Fig. 10. The overall activities of the catalysts prepared from Pd_1Zr_3 were dependent on the conditions of activation. The catalyst prepared from amorphous alloy by *in situ* activation at 698 K (a-698-is) was the most active of all investigated catalysts. Reaction rates, turnover frequencies (TOF), temperatures at which 50% of methane oxidation is attained ($T_{50\%}$), and apparent activation energies (E_a) are summarized in Table 3. The turnover frequency calculation is based on the moles of carbon dioxide produced at 520 K per second per mole of surface

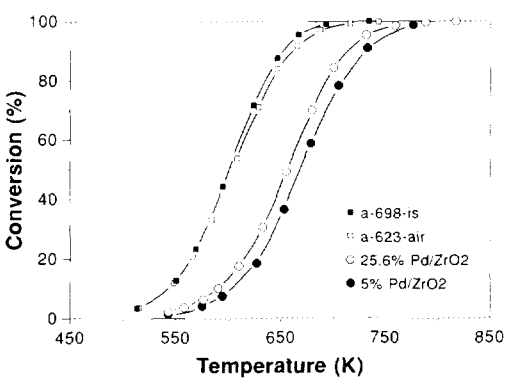

FIG. 10. Comparison of the overall activities of catalysts a-698-is, a-623-air, 5% Pd/ZrO_2, and 25.6% Pd/ZrO_2. Reactant gas composition: 1% CH_4, 4% O_2, He (balance); contact time W/F = 1120 g cat s/mol, where W (g) is the catalyst weight and F (mol/s) the total molar feed gas flow.

TABLE 3

Kinetics Results of the Investigated Catalysts under Oxygen-Rich Conditions

Catalyst	E_a[a] (kJ/mol)	$T_{50\%}$[b] (K)	Reaction rate[c] (mol/kg h)	TOF[c] (s^{-1}) $\times 10^{-3}$	m[d]	n[e]
a-573-is	97 ± 4	646	0.73	2.0	0.49	0.20
a-623-is	88 ± 1	638	0.90	2.1	0.33	0.16
a-673-is	91 ± 4	609	1.41	3.3	0.17	0.16
a-698-is	96 ± 5	600	1.21	2.9	0.29	0.18
a-723-is	97 ± 4	608	0.86	2.2	0.27	0.19
a-573-air	90 ± 1	628	0.85	2.0	0.47	0.01
a-623-air	92 ± 5	605	1.33	2.6	0.41	0.11
a-673-air	94 ± 1	617	1.18	2.3	0.34	0.10
c-673-is	94 ± 3	647	0.77	2.7	0.34	0.15
c-623-air	88 ± 2	663	0.74	2.1	0.43	−0.01
5% Pd/ZrO_2[f]	94 ± 2	669	0.17	0.8	0.79	0.01
25.6% Pd/ZrO_2[f]	76 ± 2	656	0.33	0.7	0.51	0.14

[a] Apparent activation energy with 95% confidence limits.
[b] Temperature at which 50% methane conversion was attained.
[c] Calculated at 520 K.
[d] Reaction order (m) with respect to methane, determined at 513 K and 4050 Pa oxygen.
[e] Reaction order (n) with respect to oxygen, determined at 513 K and 1000 Pa methane.
[f] After 2 h treatment at 723 K in the reactant mixture.

palladium present initially. The intrinsic activity was found to be highest with the catalysts a-673-is and a-698-is. Note that the TOF values of the catalysts prepared from Pd_1Zr_3 were more than twice as high as those of the conventionally prepared catalysts.

A comparison of the Arrhenius plots of a-698-is, a-623-air, and the two reference catalysts is depicted in Fig. 11. The apparent activation energies were found to vary between 87 and 97 kJ/mol for the catalysts prepared from Pd_1Zr_3, and for the 5 wt% Pd/ZrO_2 catalyst a value of 93 kJ/mol was determined. The catalyst prepared by coprecipitation showed a significantly lower activation energy (76 kJ/mol). These values are in good agreement with previously reported activation energies for palladium on various supports (*5*, *8*).

The dependence of the methane oxidation rate on the partial pressures of oxygen and methane, based on the empirical rate expression

$$r = kP_{CH_4}^m P_{O_2}^n,$$

has been determined for all catalysts. The reaction order with respect to methane was obtained by varying the partial pressure of methane from 410 to 3000 Pa, while keeping the mole fraction of oxygen at 4050 Pa. The order with respect to oxygen was found

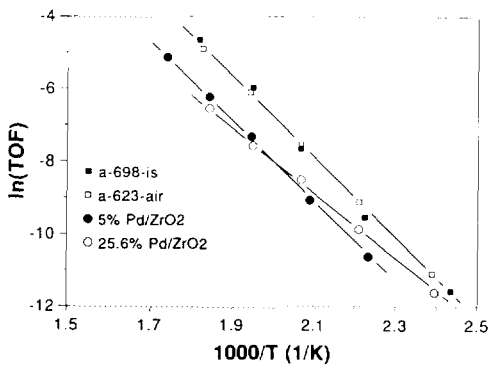

FIG. 11. Arrhenius plots for catalysts a-698-is, a-623-air, 5% Pd/ZrO_2, and 25.6% Pd/ZrO_2. Reactant gas composition, 1% CH_4, 4% O_2, He (balance); contact time W/F = 1120 g cat s/mol.

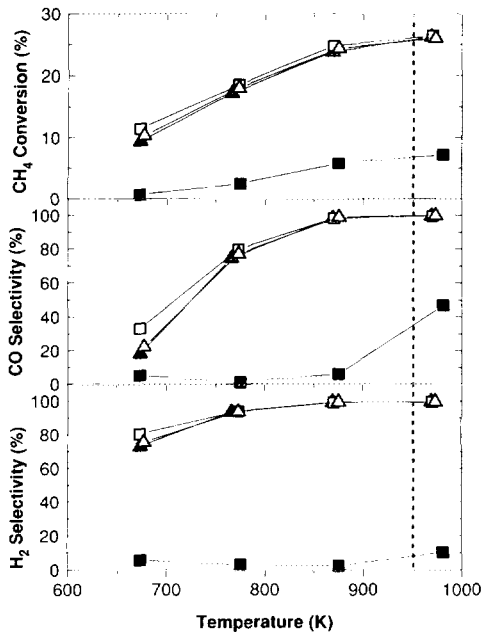

FIG. 12. Comparison of the catalytic behavior of catalysts: 5 wt% Pd/ZrO_2 (△), 25.6 wt% Pd/ZrO_2 (□), a-623-is (▲), and ZrO_2 (■). Overall activities (top), selectivities to CO (middle), and selectivities to H_2 (bottom) are plotted. Reactant gas composition, 16.64% CH_4, 2.08% O_2, He (balance); contact time W/F = 2240 g cat s/mol.

by varying the partial pressure of oxygen from 1200 to 8500 Pa, while keeping the partial pressure of methane at 1000 Pa. The orders of reaction are summarized in Table 3.

Catalytic Activity under Methane-Rich Conditions

The oxidation under reducing conditions was investigated focusing on the reaction products. The two reference catalysts and sample a-623-is were examined. With all these catalysts CO, H_2, CO_2, and H_2O were the major reaction products. Mass spectroscopy also showed a very low intensity at m/z = 27 (about 1/2500 of the intensity at m/z = 28), which could correspond to a fragmentation peak of C_2H_4. This component was neglected in the calculations.

The temperature dependences of the methane conversion and selectivities for CO and H_2 are shown in Fig. 12. It should be mentioned that at 970 K the formation of carbonaceous deposits on the reactor wall and on the catalyst was observed. Tests carried out with the empty reactor showed no carbon deposition, which hints at the possibility that palladium and/or zirconia initiated homogeneous reactions leading to the carbonaceous deposit. Since the formation of carbon was not taken into account in the carbon mass balance for the calculation of the CO selectivity, data collected at temperatures higher than 950 K should be considered with caution (Fig. 12, data beyond dashed line).

Note that high selectivities to H_2 and CO were achieved over all three catalysts. These results corroborate the high CO selectivities recently reported for supported palladium catalysts (*24*). The selectivities were improved in the presence of palladium as compared to reaction with zirconia alone (Fig. 12). Methane conversion, CO and H_2 yields of the three catalysts, pure zirconia, and the empty reactor at 873 K are compared in Table 4. The catalyst derived from Pd_1Zr_3 was less selective to CO than the two reference catalysts. This result is not surprising in view of the good properties of this catalyst for the deep oxidation of methane.

TABLE 4

Methane Conversion and Selectivity to Partial Oxidation Products at 873 K and with a CH_4/O_2 Ratio of 8

Reactor loading	Total CH_4 conversion (%)	Yield of	
		CO (%)	H_2 (%)
a-623-is	23.8	23.3	23.6
25.6% Pd/ZrO_2	24.7	24.2	24.5
5% Pd/ZrO_2	24.3	24.0	24.2
ZrO_2	5.7	0.3	0.1
None	0.9	0.0	0.0

Note. Reaction gas composition, 16.64% CH_4, 2.08% O_2, He (balance); contact inlet time, 2240 g cat s/mol.

DISCUSSION

The catalytic tests showed that amorphous or crystalline Pd_1Zr_3 without pretreatment is virtually inactive for methane oxidation. A major reason for this behavior is certainly the intrinsically very low surface area of the amorphous precursor material (<0.1 m^2/g). Exposure of the alloy to an oxygen-containing atmosphere at temperatures above 570 K was indispensable for the transformation of the inactive precursor into an active catalyst. The activity develops as a result of the drastic changes of the bulk and surface structure of the amorphous or crystalline alloys. Major changes occurring during activation are the partial crystallization of the amorphous alloy, the formation of palladium and palladium oxide particles, and the oxidation of zirconium to zirconia.

Marked differences in the bulk structure of the three investigated Pd–Zr systems have been found. As indicated by XRD, after reduction the catalysts prepared from Pd_1Zr_3 are mainly made up of relatively small and poorly crystalline particles of palladium, tetragonal, and monoclinic zirconia. The catalyst prepared by coprecipitation contained also relatively small palladium particles, but zirconia was practically X-ray amorphous, only traces of its tetragonal form being detected. On the contrary, the catalyst prepared by impregnation contained well-developed crystallites of palladium (mean size 30 nm) supported on zirconia of monoclinic and tetragonal structure.

Oxygen evolution experiments hint at the presence of two different kinds of PdO species in the impregnated catalyst, one from which oxygen evolves at ~900 K and another from which oxygen evolves at ~1020 K. For the catalyst prepared from the amorphous Pd_1Zr_3 and the coprecipitated catalyst, only one high-temperature oxygen desorption peak was observed. Recently Otto *et al.* (*25*) could identify by means of XPS two types of oxidized palladium (two chemically different entities) on γ-alumina. At low palladium loadings (0.5 wt% and less), palladium is highly dispersed and interacts with the support. The metal–support interaction appears to be crucial also in the palladium–zirconia system.

The activity per exposed palladium atom of the catalysts prepared from Pd_1Zr_3 was markedly higher than the activity of the two reference catalysts. Hicks *et al.* (*6, 26*) suggested that methane oxidation over alumina-supported palladium is a structure-sensitive reaction. They found that the TOF, based on the initial dispersion, depended strongly on the size of the palladium particles. Under their reaction conditions, small crystallites on the support were converted into dispersed PdO, while large crystallites were converted into smaller ones covered with adsorbed oxygen, which are 10 to 100 times more active than the dispersed PdO.

The 5 wt% Pd/ZrO_2 catalyst reported in this work contained large palladium crystallites (30 nm), and an increase of the activity was observed after exposure to reaction conditions. However, the intrinsic activity of the palladium species in this catalyst was lower than the activity of palladium species in the catalysts prepared from Pd_1Zr_3.

To determine if this behavior was specific for the methane oxidation, CO oxidation experiments were carried out with amorphous Pd_1Zr_3, activated under methane oxidation conditions, and the coprecipitated catalyst. The catalyst derived from Pd_1Zr_3 showed a TOF nine times higher at 303 K than that of the coprecipitated catalyst, although the palladium content of both were nearly the same.

These findings corroborate earlier studies (*14, 27*), where Pd/ZrO_2 catalysts prepared from amorphous Pd_1Zr_2 alloys by *in situ* activation under CO oxidation conditions were found to exhibit higher specific activity than similar catalyst prepared by conventional impregnation. Electron microscopy and X-ray diffraction showed that these catalysts were made up of small intergrown crystalline domains of palladium phases (Pd and PdO) and zirconia forming an extremely large interfacial area. X-ray photoelectron

spectroscopy revealed that zirconia existed as nonstoichiometric ZrO_{2-x}, in the surface and subsurface region (*27*).

The catalyst properties seem to depend significantly on intimate contact of the active constituents Pd and PdO and the zirconia as a storage and transport medium for oxide ions. This contact is achieved by a maximum interface area resulting from a disc shape of the particle for which evidence has been found in previous studies (*14, 27*). These structural features, which are not observed with the conventionally prepared catalysts, can enhance the transfer of oxygen through the ion-conducting zirconia to the active palladium phases and are suggested to contribute to the higher specific activities of the catalysts prepared from palladium–zirconium alloys, as discussed in detail in a previous work (*27*). Shyu *et al.* (*28*) showed, using XPS for Pd/CeO_2 and $Pd/CeO_2/Al_2O_3$, that CeO_2 promotes the oxidation of palladium. However, the addition of CeO_2 to Pd/Al_2O_3 retards the catalytic oxidation rate of propane over palladium for reactant mixtures, which exceed the stoichiometric oxygen/propane ratio, possibly due to a much stronger interaction between palladium and ceria than between palladium and nonstoichiometric zirconia.

The reaction order with respect to methane of 0.79 for the 5 wt% Pd/ZrO_2 catalyst is in good agreement with the order found by Yao (*7*) for unsupported palladium. However, it varied between 0.2 and 0.5 for catalysts prepared from Pd_1Zr_3 and was 0.5 for the catalyst prepared by coprecipitation. This low reaction order with respect to methane hints to a reaction mechanism in which the slowest step is the reaction of adsorbed methane with strongly adsorbed oxygen.

The most interesting result of the catalytic tests under reducing conditions was the selective oxidation of methane to synthesis gas ($H_2/CO \cong 2$) at 873 K, according to the overall reaction

$$CH_4 + \tfrac{1}{2}O_2 \rightarrow CO + 2H_2.$$

The reaction mechanism of the methane oxidation over palladium is not yet well understood. Ashcroft *et al.* (*29*) suggested a mechanism for the partial oxidation of methane on lanthanide ruthenium oxide catalysts, which is initiated by the total oxidation of methane and followed by a sequence of steam-reforming and water–gas shift reactions.

Under reducing conditions, the three different types of Pd/ZrO_2 catalysts investigated in this work yielded similar activities and selectivities (Fig. 12), which may indicate that the reaction rate was diffusion controlled under these conditions and that the product distribution was determined by the chemical equilibrium of steam reforming and water–gas shift reactions. At low temperatures, the equilibrium constant for the water–gas shift reaction

$$CO + H_2O \rightleftarrows CO_2 + H_2$$

is relatively large (8.3 at 700 K) so that part of the CO reacts with H_2O, increasing the amount of H_2. This is in agreement with the ratio H_2/CO greater than 2 observed at temperatures below 800 K.

CONCLUSIONS

Active catalysts for the methane oxidation have been prepared from an amorphous Pd_1Zr_3 alloy precursor by oxidizing it in air and *in situ*, i.e., by exposing the alloy to a CH_4/O_2 reactant gas mixture, at high temperatures. The morphological properties and catalytic activities of these catalysts were compared with those of Pd/ZrO_2 catalysts prepared by coprecipitation and by impregnation. The activity of the conventionally prepared Pd/ZrO_2 catalysts increased after aging in a reaction gas mixture containing 1% CH_4, 4% O_2, and 95% He. Under these conditions, the reaction rates (referred to the moles of Pd on the surface determined by CO chemisorption) for catalysts derived from amorphous Pd_2Zr_3 precursor were more than twice as high as those of the conventionally prepared catalysts. The different activity behavior is attributed to the ex-

tremely large interfacial area between palladium phases (Pd and PdO) and zirconia present in these catalysts, as revealed in previous studies (*14, 27*). These structural features also result in different stability of PdO with respect to decomposition as evidenced by TPD and DTA measurements.

Under methane-rich conditions, selectivities above 90% to CO and to H_2 at 870 K have been achieved on all catalysts. At higher temperatures, the reaction was influenced by the formation of carbonaceous deposits.

ACKNOWLEDGMENTS

We thank P. Wägli for the SEM investigation and Lonza AG for providing the glassy metal alloys. Financial support of this work by the Bundesamt für Energiewirtschaft (BEW) is kindly acknowledged.

REFERENCES

1. Ismagilov, Z. R., and Kerzhentsev, M. A., *Catal. Rev. Sci. Eng.* **32** (1 and 2), 51 (1990).
2. Prasad, R., Kennedy, L. A., and Ruckenstein, E., *Catal. Rev. Sci. Eng.* **26**(1), 1 (1984).
3. Trimm, D. L., *Appl. Catal.* **7**, 249 (1983).
4. Kesselring, J. P., *in* "Advanced Combustion Methods" (F. J. Weinberg, Ed.). Academic Press, London, 1986.
5. Anderson, R. B., Stein, K. C., Feenan, J. J., and Hofer, L. E. J., *Ind. Eng. Chem.* **53**, 809 (1961).
6. Hicks, R. F., Qi, H., Young, M. L., and Lee, R. G., *J. Catal.* **122**, 280 (1990).
7. Yao, Y.-F. Y., *Ind. Eng. Chem. Prod. Res. Dev.* **19**, 293 (1980).
8. Cullis, C. F., and Willatt, B. M., *J. Catal.* **83**, 267 (1983).
9. Briot, P., and Primet, M., *Appl. Catal.* **68**, 301 (1991).
10. Vernon, P. D. F., Green, M. L. H., Cheetham, A. K., and Ashcroft, A. T., *Catal. Lett.* **6**, 181 (1990).
11. Shibata, M., and T. Masumoto, T., *in* "Preparation of Catalysis IV" (B. Delmon, P. Grange, P. A. Jacobs, and G. Poncelet, Eds.). Elsevier, Amsterdam, 1987.
12. Baiker, A., *Faraday Discuss. Chem. Soc.* **87**, 239 (1989).
13. Molnar, A., Smith, G. V., and Bartok, M., *in* "Advances in Catalysis" (D. D. Eley, H. Pines, and P. B. Weisz, Eds.), Vol. 36, p. 329. Academic Press, San Diego, 1989.
14. Baiker, A., Gasser, D., Lenzner, J., Reller, A., and Schlögl, R., *J. Catal.* **126**, 555 (1990).
15. Rau, R. C., *in* "Encyclopedia of X-Rays and γ-Rays" (G. L. Clark, Ed.), p. 184. Reinhold, New York, 1963.
16. Barnickel, P., Wokaun, A., and Baiker, A., *J. Chem. Soc. Faraday Trans.* **87**, 333 (1991).
17. Massalski, T., "Binary Alloy Phase Diagrams." Am. Soc. for Metals, Metals Park, Ohio, 1986.
18. Baiker, A., Maciejewski, M., and Tagliaferri, S., *Ber. Bunsenges. Phys. Chem.* **97**, 286 (1993).
19. Mercera, P. D. L., van Ommen, J. G., Doesburg, E. B. M., Burggraaf, A. J., and Ross, J. R. H., *Appl. Catal.* **71**, 363 (1991).
20. Sing, K. S. W., Everett, D. H., Haul, R. A. W., Moscou, L., Pierotti, R. A., Rouquérol, J., and Siemieniewska, T., *Pure Appl. Chem.* **57**(4), 603 (1985).
21. Baiker, A., and Kohler, M. A., *in* "Handbook of Heat and Mass Transfer" (W. P. Cheremisinoff, Ed.), Vol. 3, p. 3. Gulf, Houston, 1989.
22. Baldwin, T. R., and Burch, R., *Appl. Catal.* **66**, 359 (1990).
23. Baldwin, T. R., and Burch, R., *Appl. Catal.* **66**, 337 (1990).
24. Bhattacharya, A. K., Breach, J. A., Chand, S., Ghorai, D. K., Hartridge, A., Keary, J., and Mallick, K. K., *Appl. Catal. A* **80**, L1 (1992).
25. Otto, K., Haack, L. P., and deVries, J. E., *Appl. Catal. B* **1**, 1 (1992).
26. Hicks, R. F., Qi, H., Young, M. L., and Lee, R. G., *J. Catal.* **122**, 295 (1990).
27. Schlögl, R., Loose, G., Wesemann, M., and Baiker, A., *J. Catal.* **137**, 139 (1992).
28. Shyu, J. Z., Otto, K., Watkins, L. H., Graham, G. W., Belitz, R. K., and Gandhi, H. S., *J. Catal.* **114**, 23 (1988).
29. Ashcroft, A. T., Cheetham, A. K., Foord, J. S., Green, M. L. H., Grey, C. P., Murrell, A. J., and Vernon, P. D. F., *Nature* **344**, 319 (1990).